We are IntechOpen, the world's leading publisher of Open Access books Built by scientists, for scientists

4,800
Open access books available

122,000
International authors and editors

135M
Downloads

Our authors are among the

154
Countries delivered to

TOP 1%
most cited scientists

12.2%
Contributors from top 500 universities

CLARIVATE ANALYTICS BOOK CITATION INDEX INDEXED

WEB OF SCIENCE™

Selection of our books indexed in the Book Citation Index in Web of Science™ Core Collection (BKCI)

Interested in publishing with us?
Contact book.department@intechopen.com

Numbers displayed above are based on latest data collected.
For more information visit www.intechopen.com

Chapter 12

Non-Linear Energy Harvesting with Random Noise and Multiple Harmonics

Ji-Tzuoh Lin, Barclay Lee and Bruce William Alphenaar

Additional information is available at the end of the chapter

http://dx.doi.org/10.5772/50727

1. Introduction

Harvesting energy from background mechanical vibrations in the environment has been proposed as a possible method to provide power in situations where battery usage is impractical or inconvenient. The most commonly used method for energy harvesting is to generate power from the vibrations of a piezoelectric material [1-3]; other methods include electromagnetic inductive coupling [4-6] and charge pumping across vibrating capacitive plates [7-10]. It has been shown that a piezoelectric cantilever attached to a vibrating structure can be used to power wireless transmission nodes for sensing applications [9]. In order to generate sufficient power, the frequency of the vibration source must match the resonant frequency of the piezoelectric cantilever. If the source vibrates at a fixed, known frequency, the dimensions of the cantilever, and the proof mass can be adjusted to ensure frequency matching. Many naturally occurring vibration sources do not have a fixed frequency spectrum, however, and vibrate over a broad range of frequencies. Lack of coupling of the piezoelectric cantilever to the off-resonance vibrations means that only a small amount of the available power can be harvested.

Recent reports have shown that the resonant frequency of a simply supported beam [11] or a piezoelectric cantilever [12] can be tuned by applying an axial force. Research also show that the resonant frequency of a cantilever can also be manipulated by applying a transverse force on the cantilever [13,14]. (In all these cases, the cantilevers response remained within the linear regime.) In principle, this effect could be developed into an active tuning scheme which matches the cantilever resonance to the maximum vibrational output of the environment at any particular time. Calculations indicate, however, that the power consumed by active tuning completely offsets any improvement obtained in the scavenging efficiency [15]. More promising are passive tuning schemes in which a fixed force modifies the frequency response of the cantilever beam, without requiring additional power input.

For example, an attractive magnetic force acting above the cantilever beam reduces the spring constant of the cantilever and lowers the resonance frequency [13,14], while an attractive force acting along the axis of the cantilever applies axial tension, and increases the resonance frequency [12]. While this can be used to tune the resonant frequency, there is no increase in output power, and the cantilever motion can even be dampened by the magnetic force and the resulting power output reduced [12,13].

The use of a magnetic force to introduce non-linear oscillation in cantilever motion has recently been reported [16-18]. A pendulum made with piezoelectric material [16] was used to study the energy output under different strengths of random Gaussian noise. An improvement of between 400% and 600% was observed compared to a standard linear oscillator. A piezomagnetoelastic structure [17] with two external magnets was studied, in which chaotic motion was observed outside the resonance frequency. It was further reported [18] that the softening response of a cantilever due to a magnetic attractor expands the response bandwidth and also increases the off resonant amplitude significantly.

Stochastic motions have been long observed with a pendulum in a repulsive magnetic field [19-20] In a generalization effort, the optimal relationship among the physical parameters for a coupling enhancement was provided in [16] [Cottone et al., 2009] using Duffing oscillator. Improvements for the non-linear system have been attributed to an advantage in the amplification of the vibration response from energy harvesters in the stochastic regime [17-18].

Here, we will first demonstrate how this capability can be used to improve power output from a broadband vibration source, having a 1/f frequency dependence (pink noise) [21]. Note that a 1/f vibration spectrum describes a vibration source in which the power spectral density of the vibration is inversely proportional to frequency. Since many naturally occurring vibration sources display a 1/f dependence, this provides evidence that the magnetic coupling could be used for more efficient energy harvesting in practical settings.

The second part of this chapter provides an in-depth study of the response of a magnetically coupled cantilever at different frequencies [22-23]. It is our observation that amplification of the cantilever output occurs not only under stochastic motion but also due to subharmonic and ultraharmonic resonance in the vicinity of the main resonant frequency. The partial solutions of subharmonic and ultraharmonic are intrinsically embedded in the magnetic coupled equation as derived in forced oscillations of weakly nonlinear systems [24]. For a particular weakly coupled cantilever experimented in this paper, maximum output is maintained at the resonant frequency through combination of ultra-harmonic components. In a singly parametric excited scan of voltage production with non-linear piezoelectric cantilever, four distinct types of efficiency improvements are observed, in which the signal is amplified above the linear cantilever operation: (1) ultraharmonic amplification below resonance; (2) stochastic amplifications in multi-frequency and multi-amplitude oscillations; (3) ultra-sub-harmonic amplification at multiple quarter frequencies; (4) sub-harmonic amplification at one-third frequencies. For data analysis, a 1-D non-linear system coupled with piezoelectric charge production is modeled to illustrate the dynamic functions.

2. Non-linear dynamics in Pink noise background

2.1. Experimental setup and vibration backgroud

Figure 1 shows the set-up for the magnetically coupled piezoelectric cantilever measurements. The cantilever is manufactured using commercially available unimorph piezoelectric discs composed of a 0.9 mm thick PZT layer deposited on a 1 mm thick brass shim (APC International, MFT-50T-1.9A1). The disc is cut into a 13 mm wide by 50 mm long strip, and clamped at one end to produce a 44 mm long cantilever. The PZT layer extends 25 mm along the length of the cantilever, and the remainder is brass only. The proof mass (including the magnet and an additional fixture that holds the magnet) weighs 2.4 gm, while the cantilever itself weighs 0.8 gm. The electrical leads are carefully soldered with thin lead wires (134 AWP, Vishay) to the top side of the PZT and the bottom side of the shim [21].

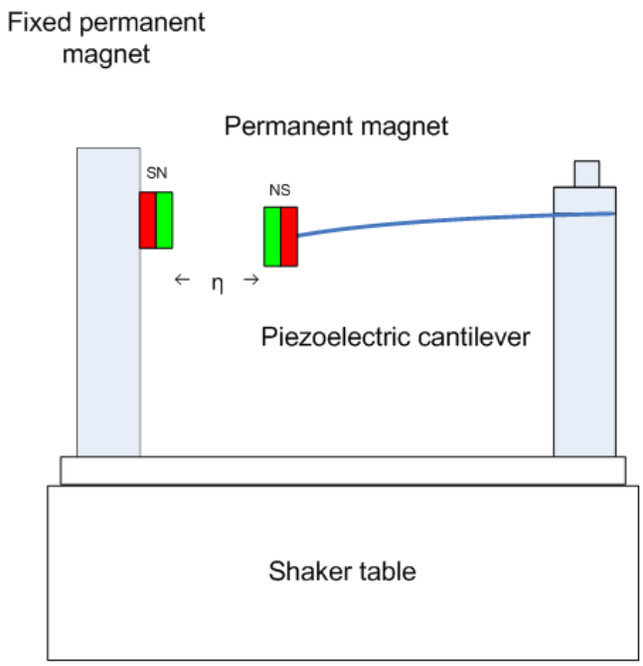

Figure 1. The experimental set-up for the magnetically coupled (non-linear) piezoelectric cantilever. The magnetic force is repulsive and bi-directional.

Vibration is generated by a shaker table (Labwork ET-126) driven by an amplified pink noise source (Labwork Pa-13 amplifier). The pink noise is generated numerically, with amplitude and crest factor set to -4dB and 1.41, respectively. The average shaker table acceleration is 7.5 m/s2, independent of the magnetic coupling. A custom Labview data acquisition program measures output voltage from the cantilever beam and the acceleration from the shaker table, once every second. The voltage peak to peak (Vpp) is measured by an oscilloscope (Agilent 54624A), and the dc voltage is detected with a digital multi-meter (YOGOGAWA 7561). A 5mm diameter round rare earth magnet (Radio Shack model 64-1895) is attached to the vibrating tip of the cantilever beam, while a similar opposing magnet is attached directly to the shaker table frame, with repulsive force. The distance between the magnets is adjusted to 5.5 mm, to make the magnetic force comparable to the spring force of the cantilever.

2.2. Experiment results

The voltage generated by the cantilever in response to the pink noise source is measured using three different circuits, (shown in Figures 2(a), 3(a), and 4(a)). In each case, the output from the coupled cantilever is compared with the output from the same cantilever in the uncoupled situation (with the opposing magnet removed). In Figure 2, the piezoelectric cantilever beam is wired directly to an oscilloscope with a 1 M Ohm input impedance and the peak-to-peak output voltage, Vpp is measured. As shown in Figure 2 (b) the cantilever output is seen to fluctuate as a function of time, reflecting the random nature of the vibrations. For much of the time, the output from the coupled and uncoupled cantilevers is similar. However, occasionally, very large voltage spikes are observed in the output from the coupled cantilever, that are not observed for the uncoupled case. The voltage peak to peak spans to 5.7 V (min. 0.7 V and max. 6.4 V) with the coupled setup and only 2.2 V (min. 0.9 V to max. 3 V) volts with the uncoupled cantilever. The overall RMS powers for the uncoupled cantilever are 3.95 μW and 4.85 μW for the coupled case. The ratio of the maximal voltage output from the coupled to the uncoupled is 2.1.

In Figure 3, the voltage generated by the piezoelectric cantilever beam is rectified, using 0.4 V forward biased diodes, and detected across a 22 μF capacitor and a 1 M Ohm resistor in parallel. As shown in Figure 3(b), the amplitude of the voltage output with this measurement circuit is most of the time higher in the coupled case than in the uncoupled case. This is because the RC decay time of the circuit is larger than the time between the large amplitude deflections of the cantilever. The average voltage measured across the capacitor or the voltage integration over time is approximately 50% higher in the coupled case.

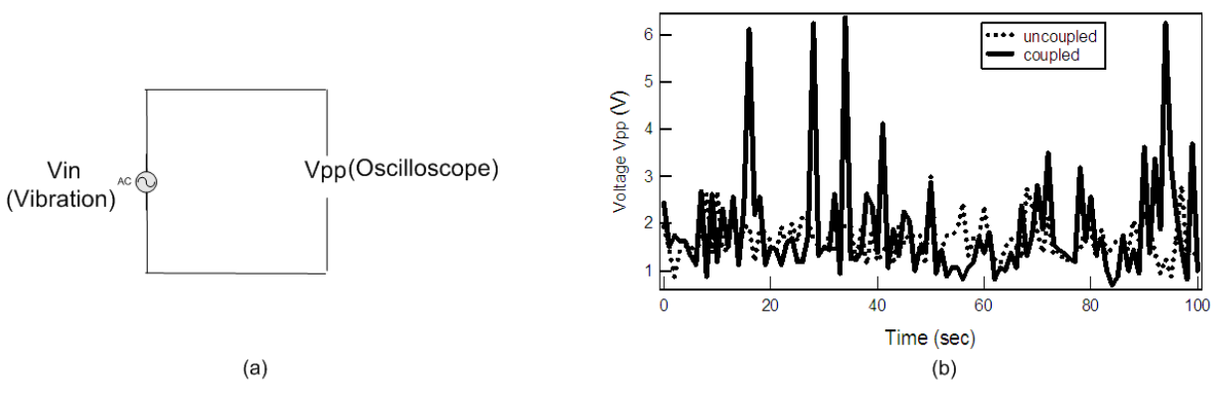

Figure 2. (a) The open circuit measurement on V_{pp} directly from the piezoelectric cantilever, and (b) the higher swing voltage reflects the voltage generated by coupling setup with larger cantilever motions.

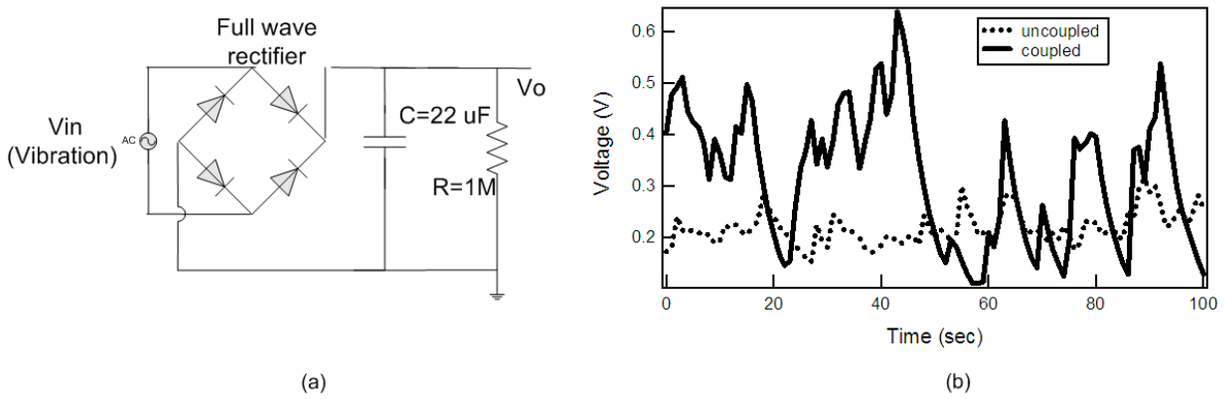

Figure 3. (a) The schematic of a rectified circuit with a 1 M Ohm resister, and (b) the fluctuations of the voltage indicate that more power being generated by the magnetic coupled cantilever.

In Figure 4, the rectified voltage is measured directly across the 22 μF capacitor without the 1 M Ohm resistor. As shown in Fig. 4(b), the voltage across the capacitor increases with time, until a maximum charging voltage is achieved. The maximum voltage measured across the capacitor is approximately 50% higher in the coupled case than in the uncoupled case. Note that there is a time delay for the coupled cantilever to achieve a higher voltage than the uncoupled cantilever. This is due to the time passing before the first large amplitude deflection occurs. The random nature of the motion means that this time will vary from run to run, however, on average the coupled cantilever output will be consistently higher than the uncoupled output. Note that in addition to producing more power, the higher voltage output enables circuit operation without a step-up transformer, eliminating the power loss in the transformer.

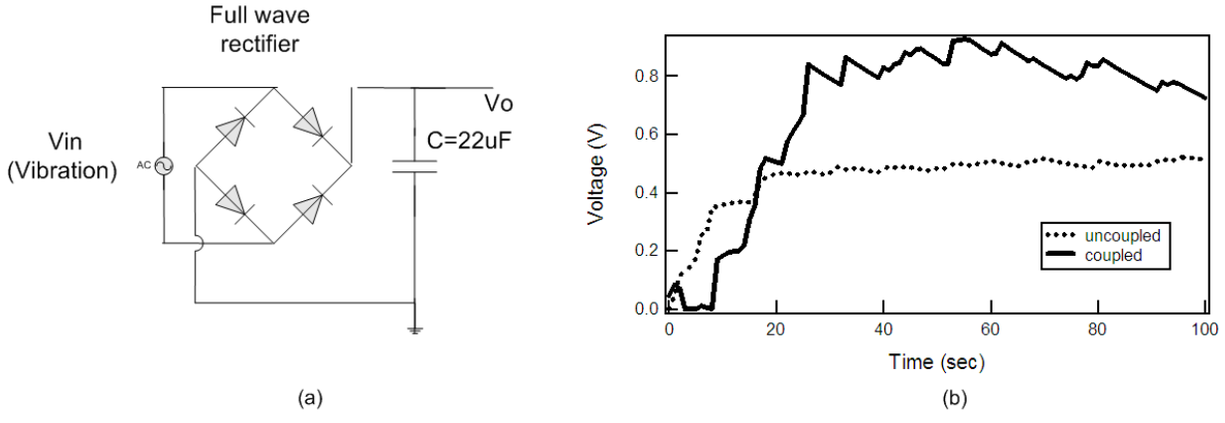

Figure 4. (a) The schematic of the storage circuit, and (b) DC voltage output measured on the storage capacitor indicating more charge is stored with the magnetic coupling setup.

2.3. Discussion

It is instructive to compare the force exerted on the cantilever in the coupled and uncoupled cases. To do this, an empirical measure of the magnetic force is obtained using the experimental set-up shown in Figure 5.

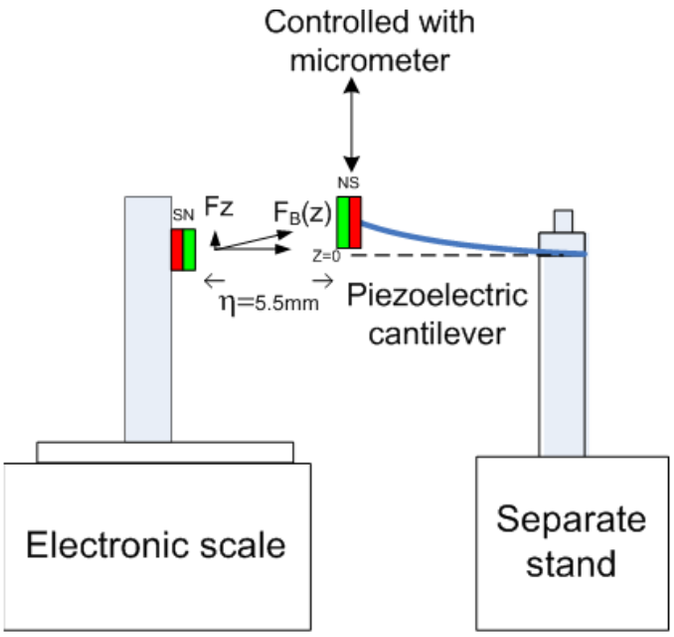

Figure 5. The magnetic force component function, F_z, is determined by the electronic scale versus the manual deflection of the cantilever.

The opposing magnet is mounted onto a measurement scale, and the position of the magnetized cantilever is manipulated by pushing up and down at the end of a cantilever beam, simulating flexure movement. The deflection z is measured using a micrometer, while the reading on the scale provides the force between the two magnets. The details of the force measurments were shown in [22]. Only the magnetic force in the z direction, F_z, contributes to the resultant spring force. At z=0, the force is zero in the z direction because the two magnetic forces only repel each other in the longitudinal direction. F_z increases as the angles between the two magnets increase until the overlap between the two magnets is zero. At this point, F_z decreases with increasing distance because the force is inversely proportional to the distance squared.

The spring force, the magnetic force and the resultant force (spring plus magnetic) are plotted in Figure 6,

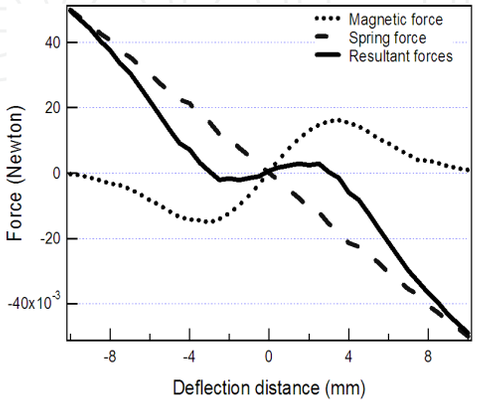

Figure 6. The plot shows the magnitude of the magnetic forces exerted on the cantilever beam, the spring forces and the resultant forces.

The resultant force is significantly reduced compared to the bare spring force near z=0. The coupled system has three equilibrium points where the resultant force is zero, compared to the single equilibrium point of the bare spring force. Because the resultant force in the region of the three equilibrium points is relatively small, transitions between the three points occurs relatively easily. Note that the middle equilibrium is unstable, therefore when the piezoelectric cantilever is set up for the coupling experiment, the cantilever is off the equilibrium point toward ground in static state as shown in Figure 1. In Figure 7 the potential energy is plotted for both the uncoupled and coupled systems. The potential energy is calculated by direct integration of the force with respect to the displacement, z. This gives for the uncoupled case, and for the coupled case. For the coupled case, the resultant potential is raised, with two local minima symmetric to z=0. This double well structure allows easy movement of the cantilever beam even when excited by non resonant forces. Once it passes the local high potential, it drifts to the other side of the balance, resulting in an increased total deflection distance. This can be seen by considering the possible motion of the cantilever beam having a kinetic energy, h, which is large enough to surmount the potential barrier at z=0. With the same random acceleration background the coupled cantilever can travel further distance than the uncoupled one. The voltage output, which depends on the movement of the cantilever, therefore, increases. The ratio of the maximum displacement in the coupled and uncoupled systems determined from Figure 7 is 2.4. This is comparable to the ratio of maximum voltage output in the coupled and uncoupled systems, which was seen in Figure 2 (b), at 2.1.

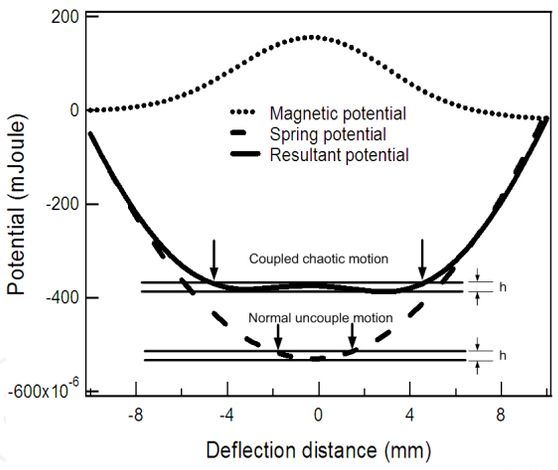

Figure 7. The direct integration from the measured forces function in Fig. 6 leads to the magnetic potential, spring potential and the resultant spring potential. The responding range in the coupled and the uncoupled cantilever is defined by the same potential height, h.

The magnetic coupling (although a passive force requiring no energy) introduces a symmetric force which acts in the opposite direction to the spring force around z=0. Being comparable in magnitude to the spring force, the magnetic force compensates the spring potential, and introduces a double valley in the potential energy profile. Under the influence of the modified spring potential, the magnetically coupled cantilever responds to a random vibration source (like the pink noise) by moving chaotically between the two minima in the

potential energy profile. As compared with the non-chaotic motion of the uncoupled cantilever around the single z=0 potential minimum, this produces larger cantilever deflection and more voltage output from the piezoelectric cantilever. The oscillations around the resonance frequency are unstable and chaotic, but persistent. The modified spring potential is higher, and flatter than the bare spring potential, making the magnetic coupled cantilever easier to excite in the random frequency region. The experiments show that the ratio of the open circuit peak to peak voltage output and the potential well are closely related. Future work includes the design and implementation of modified potential wells and further analysis of the gain due to the modified potential wells.

3. Resonance broadening in broad band spectrum

3.1. Experiment setup

The experiment set up is the same as Figure 1. In all measurements, the shaker table acceleration is set to approximately 4.2 m/s^2 at resonant freqeuncy, and the frequency swept from 0 to 30 Hz in 0.5 Hz steps. The opposing magnet fitted at the free end of the cantilever supplies a symmetrical, repulsive force about the balance of the cantilever during vibration. The horizontal separation between the magnets (designated by η) is adjusted to be approximately between 6 to 6.5 mm. This separation is found to provide the best compensation for the spring force, and makes the effective restoring force as small as possible near the equilibrium point.

3.2. Experiment result with open circuit

Figure 8 shows both the output of the piezoelectric cantilever as a function of shaker table vibration frequency for the linear and non-linear case. The voltage generated by the piezoelectric cantilever beam is directed measured by oscilloscope treated as an open circuit. At the resonance frequency (measured to be 9.5 Hz) the output of the cantilever was 53 V, and the peak height, resonance frequency and line width are all approximately the same for the linear and non-linear states (here linear refers to the non-coupled state, while non-linear refers to the magnetically coupled state). On either side of the main resonance, however, there is additional output observed for the non-linear cantilever, which is not observed in the linear state. As can be seen from a comparison of the linear and the non-linear runs, the overall amplitude profile of the non-linear run is much larger in the sense of a broadband distribution, although there are gaps between peaks in the overall pattern of the non-linear output.

Figure 9 shows the output of both the linear and non-liner cantilever measured as a function of time at selected frequency to illustrate the comparison of the linear and non-linear dynamics. The voltage output of the non-linear cantilever evolves with frequency, while being amplified close to the resonance frequency. The spectrum shows a variety of amplified motions and harmonics. For example, at a driving frequency as low as 6.5 Hz (between 6-7.5Hz) (Figure 9(a)) both the linear and non-linear cantilever motions follow the

vibrations of the shaker table, producing periodic oscillations. The amplitude of the oscillations for the non-linear cantilever is 5 times larger than those for the linear cantilever, however. At the resonant frequency (Figure 9(b)) both linear and non-linear cantilevers oscillate at the driving frequency with equal amplitudes. At 13 Hz (Figure 9(c)) the linear cantilever motion continues to follow the vibrations of the shaker table, producing low amplitude periodic oscillations. The non-linear cantilever motion is aperiodic and has a magnitude which is on average 3 times larger than that of the linear cantilever. At 16 Hz (Figure 9 (d)) the non-linear cantilever produces a 3 times larger peak to peak amplitude than the linear cantilever, and shows multiple and periodic "half-way" vibrations. At 20Hz (Figure 9 (e)) the non-linear cantilever shows a 5 times larger amplitude at the frequency of 6.7Hz than the linear output at 20 Hz.

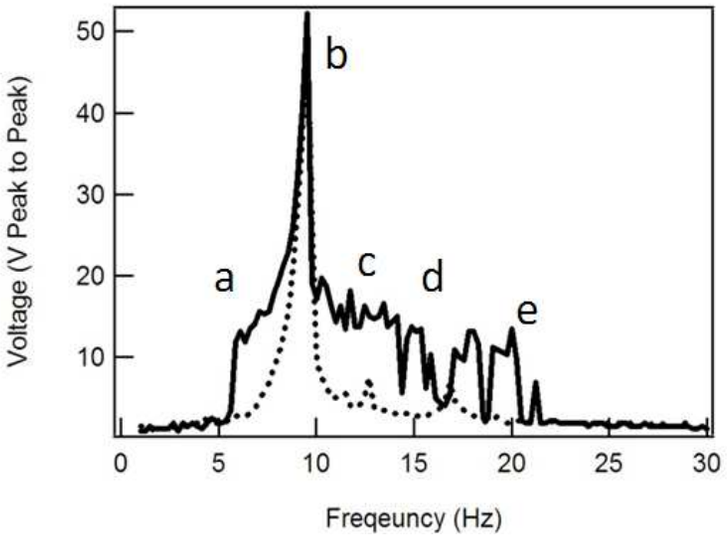

Figure 8. The voltage output (peak to peak) of the piezoelectric cantilever measured as a function of frequency (dash line for linear and solid line for non-linear state).

Note should be taken that there are two unexpected small peaks at 12.5 Hz and 17 Hz for the linear response. The peaks at 12.5 Hz and 17 Hz on the experiment data come from the torsion and standing wave oscillations. It is the result of how the piezoelectric cantilever was facilitated with magnet and its fixture as the proof mass. The cantilever is relatively thin and droops naturally due the weight of proof mass a few millimeters (as shown in Figure 1) to a curve. The L-shape fixture that holds the magnet was bolted with a screw on one side parallel to the brass shim. The magnet is then attached on the other side of the L-shape fixture, perpendicular to the brass shim in such way to make magnetic coupling. During the process, the cantilever was deformed and twisted slightly. As a result, the combined proof mass is slightly located off the center of the cantilever beam resulting in weight imbalance and torsion mode resonance. The fixture also creates an area where the free end is rigid with the fixture, which acts like a semi-fixed end, paving a way for a standing wave vibration when the cantilever is excited. Finite Element Analysis (FEA) simulating the structure and dimensions confirms that the first 3 modes of vibration include bending, torsion and standing wave oscillations.

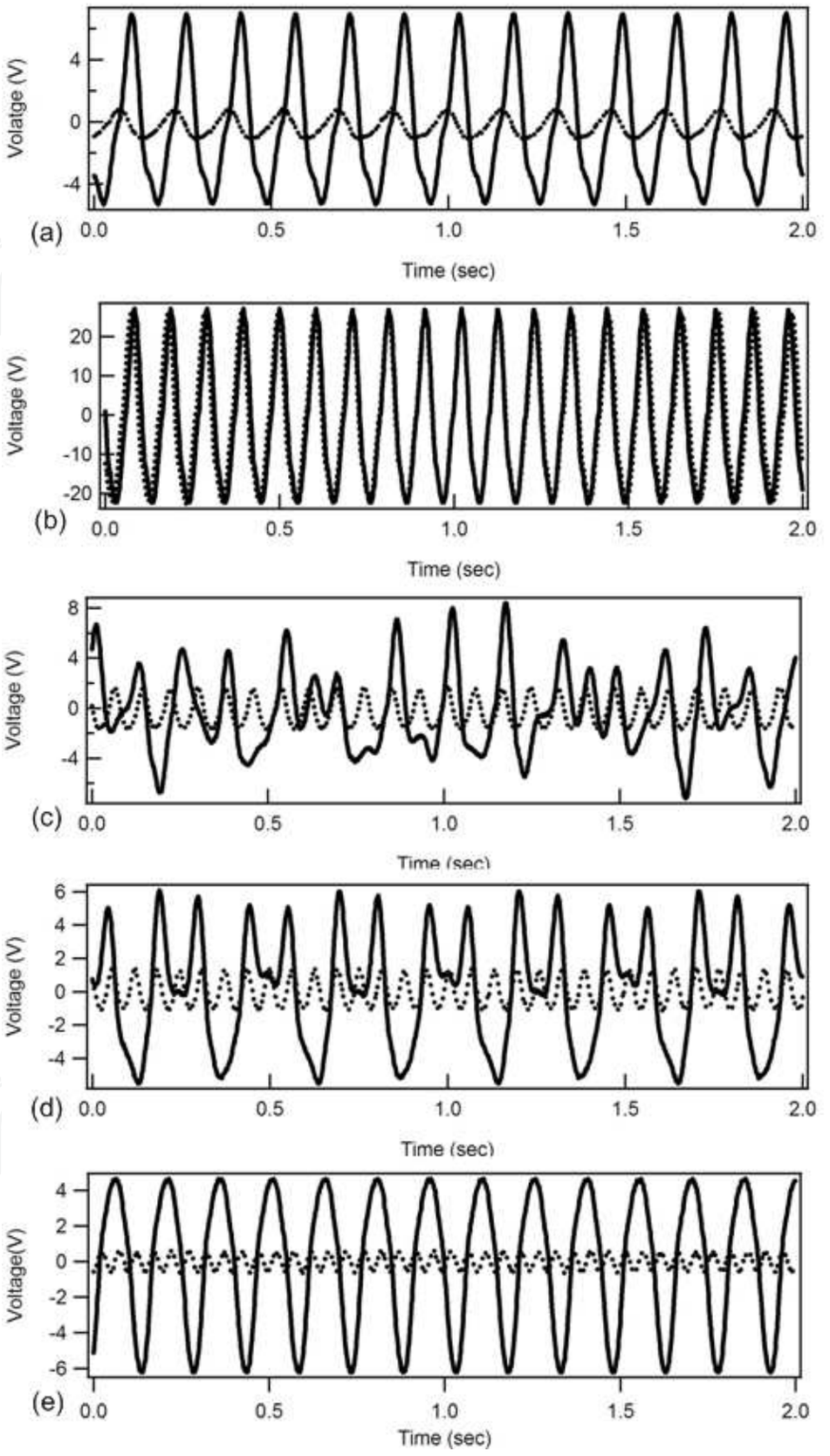

Figure 9. The output of the linear (dash line) and non-linear (solid) system in the time domain: (a) 6.5 Hz (b) 9.5Hz at resonance; (c) 13 Hz ; (d) 16Hz ;(e) 20Hz

3.3. Theoretical simulations

The dynamics of the piezoelectric cantilever is modeled by a 1-D driven spring-mass system coupled with the piezoelectric effect under the influence of a magnetic force Fm(z) [17-18]:

$$m\ddot{z} + d\dot{z} + kz + F_m(z) + \sigma V = mA(\omega)cos(\omega t), \tag{1}$$

with mass m=0.0024 kg, damping coefficient d=0.0075 kg/sec, spring constant k=8.55 N/m, and angular frequency ω. Here, z is the vertical deflection of the cantilever, V is the generated voltage, σ=5x10-6 N/V is the coupling coefficient, and A is the acceleration of the shaker table (A=4.2 m/sec2 measured at resonance frequency). The voltage output is related to the deflection of the piezoelectric cantilever through:

$$\dot{V} + \frac{1}{R_l C_l} V + \theta \dot{z} = 0 \tag{2}$$

where R_l is the equivalent resistance, C_l is the equivalent capacitance and 1/ (R_l C_l)= 0.01 , and θ=1250 is the piezoelectric coupling coefficient in the measured circuit. The transverse magnetic force (in the z direction) is determined from the force between two magnetic dipoles (Kraftmakher, 2007):

$$F_m(z,\eta) = \frac{-3u_0 M^2 a(bz)(4\eta^2 - (bz)^2)}{4\pi((bz)^2 + \eta^2)^{\frac{7}{2}}} \tag{3}$$

where M is the dipole magnetization, u0 is the permeability in air, and η is the horizontal separation between the magnets at z=0. The correction factors a and b are included to compensate for the flexure motion of cantilever and the magnetic force along the cantilever axis [16]. The magnetization M is determined by direct measurement of the axial force between the cantilever and a fixed magnet using a reference scale [22].

The solution to the coupled differential equations (1) and (2) is determined using Maple software to give the voltage output versus time for a given driving frequency, magnetic force function, and separation η. In order to fit our experiment data, the magnetic force Fm(z) was modified by a and b parameters and used for our calculation, where M = 0.011Am2, η = 6.5 mm, a = 1.04 and b = 1.21. As in the experiment, the output is calculated for t = 0 to 10 seconds, and the maximum peak-to-peak output over the last 2 seconds obtained. The result of the frequency domain is showed in Figure 10, which resembles the experimental result as seen in Figure 8.

Both the experiment and simulation figures show broadband vibration for the non-linear configuration between 6-20Hz. The simulation in Figures 11(a)-(e) reproduces many of the features observed in the experiment in Figures 9(a)-(e). The rest of Figures 11-15 reveals more about the complexity of the multiple harmonics in the non-linear systems. The simulations of the time domain with the corresponding frequency selected from experiment are shown in Figures 11(a)-15(a). Figures 11(b)-15(b) illustrate the velocity vs. voltage output

of the piezoelectric cantilever in both the linear and non-linear cases. Figures 11(c)-15(c) are the Fourier transform of the coupled cantilever cases in Figures 11(a)-15(a), respectively, showing the compositions of frequency components for the non-linear states. The following section will discuss the multiple harmonic components directly derived from the non-linear dynamics simulations.

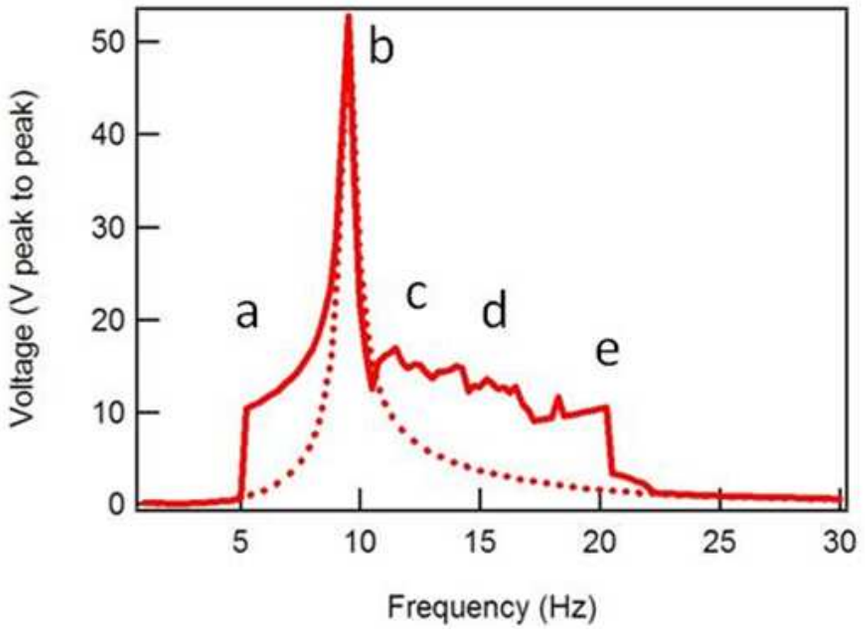

Figure 10. The simulated voltage output (peak to peak) of the piezoelectric cantilever is plotted in the frequency domain (dash line for linear and solid line non-linear).

3.4. Multiple harmonics analysis

At a driving frequency of 6.5 Hz, as seen in Figure 11(a), both the linear and non-linear cantilever motion follow the vibrations of the shaker table, producing periodic oscillations. The amplitude of the oscillations for the coupled cantilever, however, is approximately 5 times larger than those for the linear cantilever, as seen in the experiment in Figure 9(a). The velocity vs. voltage in Figure 11(b) shows that the coupled cantilever has non-linear component in voltage production. Further analysis through Fourier transformation indicates that the non-linear cantilever shows the combination of the excited 6.5 Hz harmonic (dominant and high amplitude) and the 20 Hz ultraharmonic (3 times the excited frequency), as seen in Figure 11(c).

At the resonant frequency of 9.5 Hz (Figure 12(a)) both non-linear and linear cantilevers oscillate at the driving frequency with equal amplitude of voltage output. The responses for both the coupled and uncoupled cantilever at resonant frequency are almost identical in the voltage output. The velocity vs. voltage in Figure 12(b) shows a little non-linearity at 90^{o} and -90^{o} of the vibration cycles. Through Fourier transformation as seen in Figure 12(c), the non-linear cantilever shows some components of vibration at the excited 9.5 Hz harmonic (dominant) and the 29 Hz ultraharmonic (3 times the excited frequency).

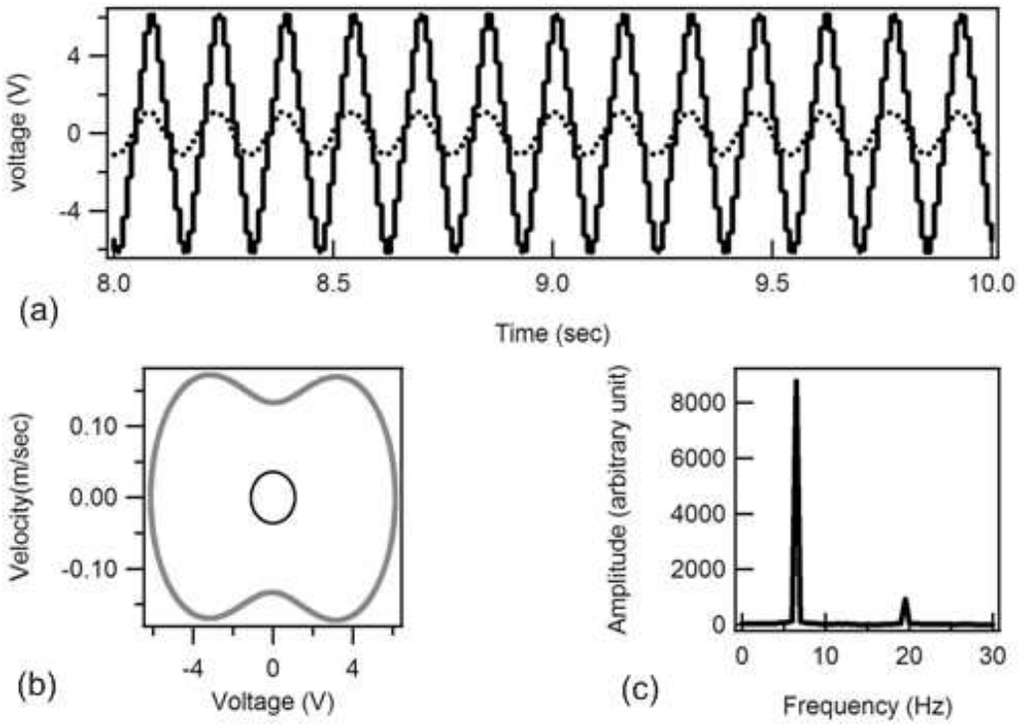

Figure 11. The theoretical analysis of excited frequency at 6.5 Hz. (a) the time domain voltage output, dash line for linear and solid line for non-linear states; (b) the velocity vs. voltage output, dark line for linear and light line for non-linear state; (c) the Fourier transform of the non-linear state from the data of Figure 5(a).

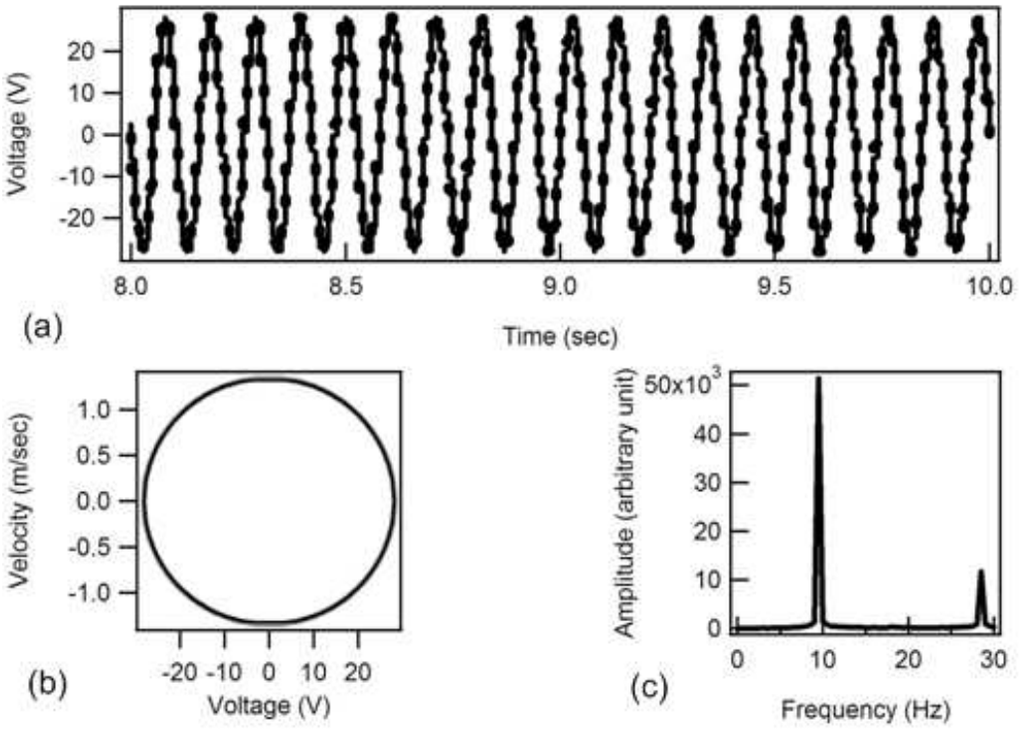

Figure 12. The theoretical analysis of excited frequency at 9.5 Hz. (a) the time domain voltage output, dash line for linear and solid line for non-linear state; (b) the velocity vs. voltage output, light line for linear and dark line for non-linear state; (c) the Fourier transform of the non-linear state from the data of Figure 12(a).

The response for the non-linear cantilever is chaotic at 13 Hz as seen in Figure 13(a), but with average 3 folds larger magnitude than the linear one. The velocity vs. voltage relation in Figure 13(b) shows chaotic motions for the coupled cantilever. Using Fourier transformation for Figure 13(a) results in Figure 13(c), the coupled cantilever shows the linear response of a small portion of 13 Hz component combined with a large amplitude distribution at lower frequency that are attributed to the chaotic motion. Note that the small peaks at 12.5 Hz and 17 Hz are not observed in the simulation as seen and discussed in the experiment section. This small torsion and standing wave bending resonance are not accounted for by the simplified 1-D model used to simulate the spring mass damping model such as an ideal cantilever.

At 16Hz, the non-linear cantilever is periodic (Figure 14(a)) and is 3 times larger (peak to peak) in magnitude than the uncoupled one, with double prone of low frequency in the upper cycle. Apparently, it is and composed of different frequency and multiple haromonic motion, with large magnitude than the uncoupled motion. The evidence is also shown in the velocity vs. voltage relationship in Figure 14(b), where 3 different cyclic loops are identifiable. Fourier transformation from time data in Figure 14(a) proves that the non-linear cantilever delivers ultra-sub-harmonic vibration at n*(16/4) Hz, where, n=integer in Figure 14(c).

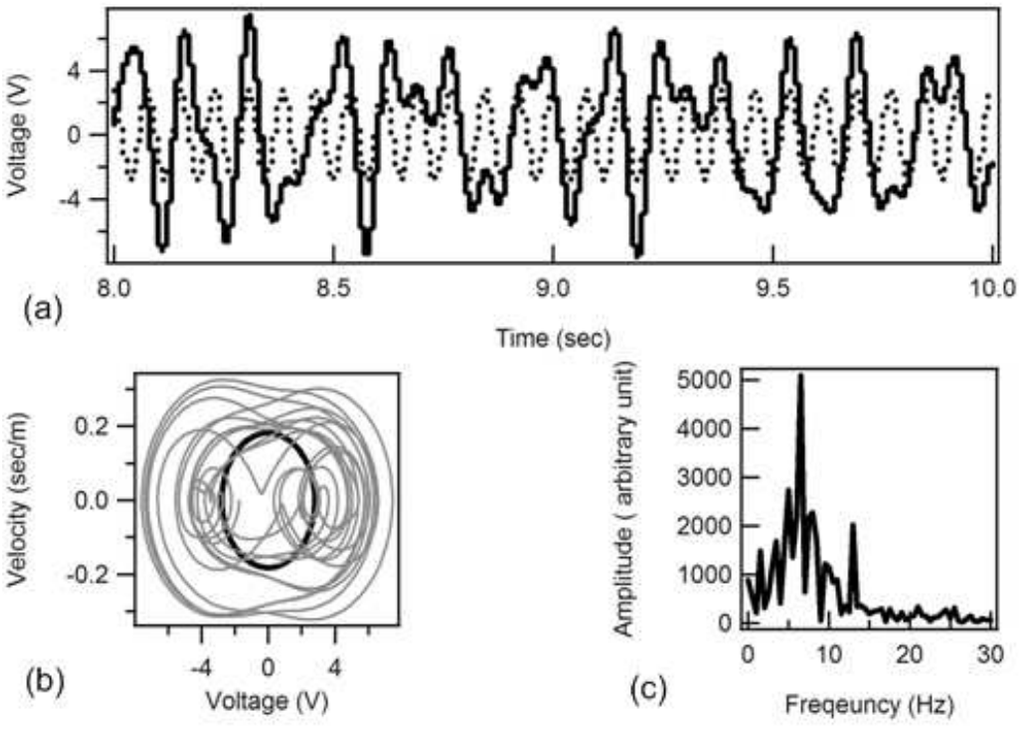

Figure 13. The theoretical analysis of excited frequency at 13 Hz. (a) the time domain voltage output, dash line for linear and solid line for non-linear states; (b) the velocity vs. voltage output, light line for linear and dark line for non-linear state; (c) the Fourier transform of the non-linear state from the data of Figure 13(a).

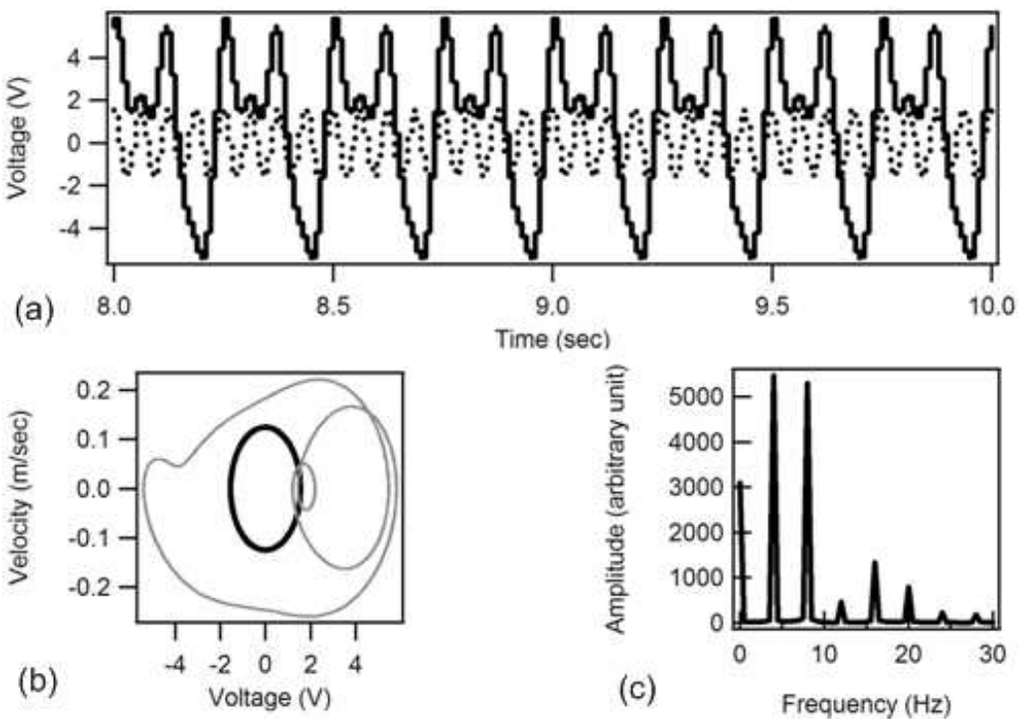

Figure 14. The theoretical analysis of excited frequency at 16 Hz. (a) the time domain voltage output, dash line for linear and solid line for non-linear states; (b) the velocity vs. voltage output, light line for linear and dark line for non-linear state; (c) the Fourier transform of the non-linear state from the data of Figure 14(a).

At 20Hz, the response for the non-linear cantilever is periodic and also 3 folds larger peak to peak magnitude than the linear one as seen in Figure 15 (a). The velocity vs. voltage in Figure 15(b) shows some combination of cyclic motions for the non-linear cantilever. Through Fourier transformation, the coupled cantilever shows subharmonic at 6.7 Hz (dominant), excite frequency/3, and 20 Hz in Figure 15(c).

The combination of the stochastic and various harmonic features have three to five folds greater voltage production than the linear standard narrow band piezoelectric cantilever. Together with the un-damped resonant response enhance the performance well beyond that of a standard energy harvester.

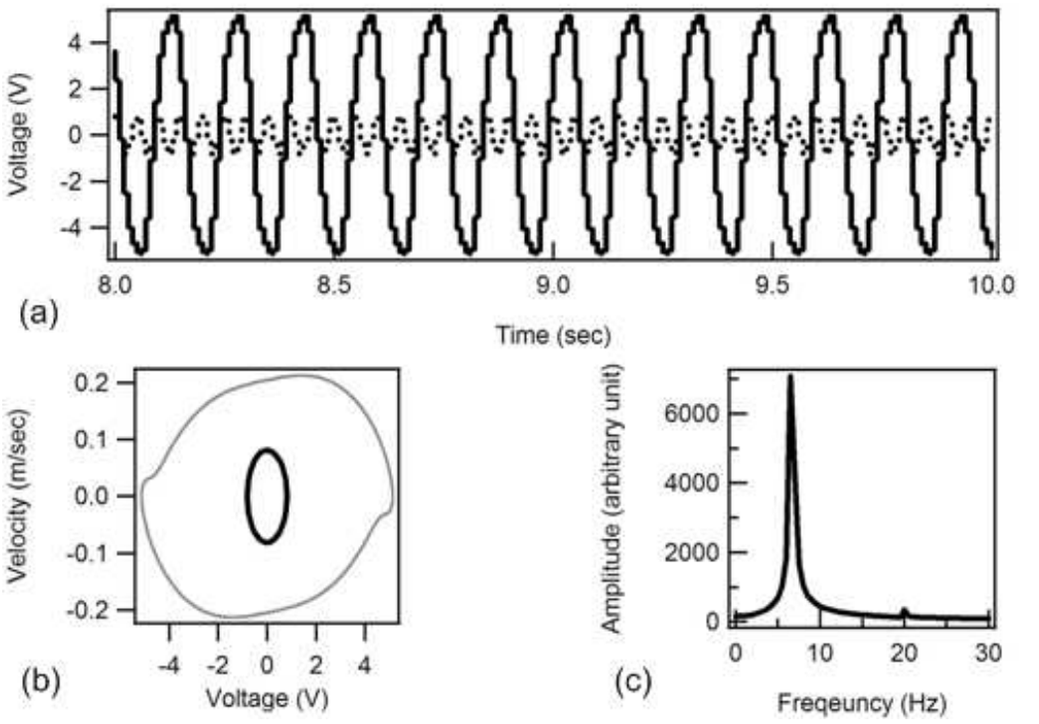

Figure 15. The theoretical analysis of excited frequency at 20 Hz. (a) the time domain voltage output, dash line for linear and solid line for non-linear states; (b) the velocity vs. voltage output, light line for linear and dark line for non-linear state; (c) the Fourier transform of the non-linear state from the data of Figure 15(a).

3.5. Experience result with storage capacitor

Figure 16 (a) shows the output of the other PZT cantilever with similar specs as a function of shaker table vibration frequency for the case where the opposing magnet is fixed to the shaker table. The voltage generated by the piezoelectric cantilever beam is rectified, and detected across a 22 μF capacitor and 1 M Ohm resistor in parallel, using the circuit shown in Figure 3 (a). The results from two measurement runs in the coupled state are shown, together with the output of the cantilever measured in the uncoupled state. (This is obtained by removing the opposing magnet.) At the resonance frequency, (measured to be approximately 10 Hz) the output of the cantilever exceeds 16 V, and the peak height, resonance frequency and linewidth are all approximately the same for the coupled and uncoupled states. On either side of the main resonance, however, there are additional output observed for the coupled cantilever, which is not observed in the uncoupled state. As can be seen from a comparison of the two coupled runs, the frequency distribution of the peaks are the result of the multiple harmonics, as predicted in the open circuit.

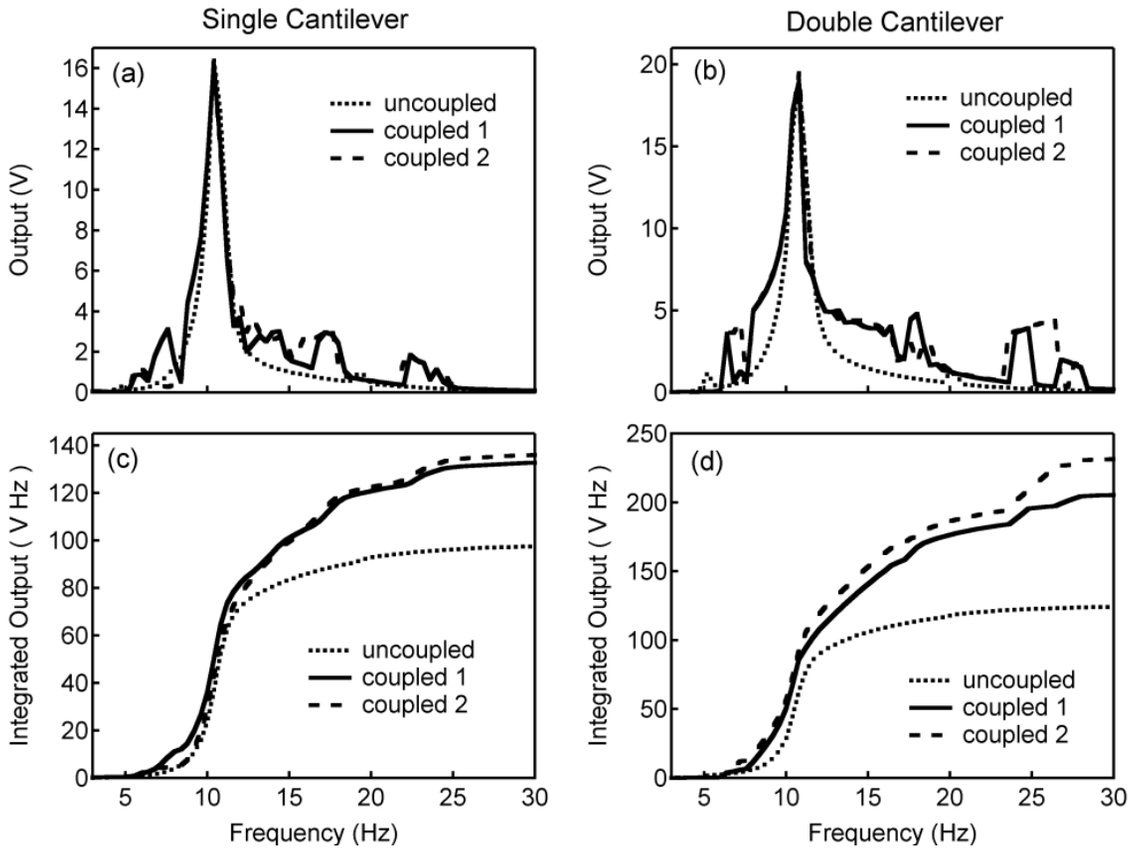

Figure 16. Voltage output of the piezoelectric cantilever as a function of shaker table frequency for **(a)** single cantilever **(b)** double cantilever. Integrated voltage output as a function of frequency for **(c)** single cantilever and **(d)** double cantilever.

Also measured was a double cantilever system, (as shown in Fig. 16(b)), in which the second magnet is connected to an opposing cantilever (having resonant frequency of around 60Hz) rather than to a fixed point. As shown in Fig. 16 (b), the results are similar to the single cantilever system, except that the double cantilever system shows a larger overall increase in off-resonance output. The overall improvement in the harvesting efficiency can be illustrated by plotting the integrated voltage output of the cantilever beam as a function of frequency. For both the single (Fig. 16 (c)) and double (Fig. 16 (d)) cantilever systems, the integrated voltage output over the 0-30 Hz bandwidth shows a substantial increase in the coupled versus the uncoupled case. The total improvement is 31%-87%, with some variation between measurement runs.

4. Conclusion

Piezoelectric cantilevers have been widely studied for energy scavenging applications, but suffer from poor output power outside of a narrow frequency range near the cantilever resonance. In this chapter, we have demonstrated how power output can be enhanced by applying a simple passive external force. When a symmetrical and repulsive magnetic force is applied to a piezoelectric cantilever beam to compensate the cantilever spring force, this lowers the spring potential and increases the output when driven by a random pink noise

vibrational source. The principle may be applied to other vibration energy harvesting devices such as electromagnetic and capacitive types in random naturally pink noise environments.

In the parametrically excited piezoelectric cantilever experiments, linear and non-linear performances were compared. Overall, four distinct types of efficiency improvements appear in the non-linear configuration, in which the signal is amplified above the linear cantilever response: low frequency ultraharmonic amplification; stochastic amplifications in multi-frequency and multi-amplitude oscillations; ultra-sub-harmonic amplification at multiple quarter frequencies; subharmonic amplification at one-third frequencies. Taken together, the stochastic, sub-harmonic and ultra-harmonic response produces an average of three to five-fold increase in voltage production. For energy harvesting purposes, the combination of the four features together with the un-damped resonant response enhances the performance well beyond that of a standard energy harvester. Furthermore, an analytical model of the bi-stable dynamics produces results consistent with those observed experimentally. The simulation tool could be deployed in the future investigation for non-linear energy harvester design for broadband and beyond natural harmonic applications.

Author details

Ji-Tzuoh Lin* and Bruce William Alphenaar
Department of Electrical and Computer Engineering, University of Louisville, Louisville, KY, USA

Barclay Lee
Department of Bioengineering, California Institute of Technology, Pasadena, CA, USA

Acknowledgement

The effort was funded by the Department Of Energy DE-FC26-06NT42795 and the U.S. Navy under Contract DAAB07-03-D-B010/TO-0198. Technical program oversight under the Navy contract was provided by Naval Surface Warfare Center, Crane Division.

5. References

[1] Elvin NG, Elvin A and Choi D 2003 A self-powered damage detection sensor J. Strain Anal. Eng. Des. 38 115-24
[2] Ottman G K Hofmann H F and Lesieutre G A 2003 Optimized piezoelectric energy harvesting circuit using step-down converter in discontinuous conduction mode IEEE Trans. Power Electron. 18 696-703
[3] Roundy S 2004 A piezoelectric vibration based generator for wireless electronics, Smart Mater. Struct. 13 1131

* Corresponding Autor

[4] Kulah H. and Najafi K. 2004, An electromagnetic micro power generator for low-frequency environmental vibrations, 17th IEEE Int. conf. Micro Electro Mechanical System, 1004 (MEMS '04) pp 237-40

[5] von Büren T and Tröster G, Design and optimization of a linear vibration-driven electromagnetic micro-power generator, Sens. Actuators A 135 (2007) 765-775

[6] S P Beeby, R N Torah, M J Tudor, P Glynne-Jones, T O'Donnell, C R Saha and S Roy, A micro electromagnetic generator for vibration energy harvesting, J. Micromech. Microeng. 17 (2007) 1257–1265

[7] Hsi-wen Lo and Yu-Chong Tai, Parylene-based electret power generators, J. Micromech. Microeng. 18 (2008) 104006-104014

[8] Sterken T, Fiorini P, Baert K, Puers R, and Borghs G, An electret-base electrostatic micro-generator transducers, The 12th International Conference on Solid State Sensors, Actuators and Microsystems. Boston, June 6-12, 2003 pp 1291-1294

[9] Shad Roundy, Paul Kenneth Wright and Jan M. Rabaey, Energy scavenging for Wireless Sensor Networks with Special Focus on Vibrations, Kluwer Academic Publishers, 2004.

[10] Y Chiu and V F G Tseng, A capacitive vibration to electricity energy converter with integrated mechanical switches, J. Micromech. Microeng. 18 (2008) No 10 104004-10412

[11] Eli S Leland and Paul K Wright, Resonance tuning of piezoelectric vibration energy scavenging generators using compressive axial preload. *Smart Mater. Struct.*15 (2006) 1413-1420

[12] Dibin Zhu, Stephen Roberts, Michael J. Tudor, and Stephen P. Beeby, Closed Loop Frequency Tuning of a Vibration-Based Microgenerator, Proceedings of PowerMEMS 2008/microEMS2008, November 2008.

[13] Vinod R Challa, M G Prasad, Yong Shi and Frank T Fisher, A vibration energy harvesting device with bidirectional resonance frequency tunnablity. *Smart Mater. Struct.*17 No 1 (2008) 015035

[14] Ji-Tzuoh Lin, Walter Jones, Bruce Alphenaar, Yang Xu and Deirdre Alphenaar. Passive magnetic coupling for enhanced piezoelectric cantilever response for energy scavenging applications. 17th International Symposium on Applications of Ferroelectrics (ISAF 2008 EH017) Feb 24-27 2008

[15] Shad Roundy and Yang Zhang, Toward self-tuning adaptive vibration-based microgenerator, Proceedings of SPIE Volume 5649 Smart Structure, Devices and System II February 2005 pp.373-384

[16] F. Cottone, H. Vocca, L. Gammaiton, Non-linear Energy Harvesting, Physical Review Letter,102, 080601 2009

[17] A. Erturk, J. Hoffmann, D. J. Inman, A piezomagnetoleastic structure for broadband vibration energy harvesting, Applied Physics Letter, 94 254102 2009

[18] Samuel C. Staton, Clark C. Mcgehee, Brian P. Mann, Reversible hysteresis for broadband magnetopiezoelastic energy harvesting, Applied Physics Letter, 95, 174103 2009

[19] Duchesne, B., C.W. Fischer, C.G. Gray, and K. R. Jeffrey. "Chaos In The Motion of An Inverted Pendulum: An Undergraduate Laboratory Experiment," Am. J. Phys. 1991; 59 (11)

[20] A. Siahmakoun, V. A. French, and J. Patterson. "Nonlinear Dynamics of A Sinusoidally Driven Pendulum In a Propulsive Magnetic Field," Am. J. Phys. 1997; 65 (5)

[21] Ji-Tzuoh Lin and Bruce Alphenaar. "Enhancement of Energy Harvested from a Random Vibration Source by Magnetic Coupling of a Piezoelectric Cantilever," Journal of Intelligent Material Systems and Structures, 2010; Vol. 21 Issue 13, 1337-1341

[22] Ji-Tzuoh Lin, Barclay Lee, and Bruce Alphenaar. "Magnetic Coupling of Piezoelectric Cantilever for Enhanced Energy Harvesting Efficiency" Smart Mater. Struct. 2010; 19 045012

[23] Ji-Tzuoh Lin, Kevin Walsh and Bruce Alphenaar. Enhanced Stochastic, Subharmonic and Ultraharmonic Energy Harvesting, Journal of Intelligent Material and Structure Systems,(accepted May 4th on line) 2012

[24] A. Prosperetti "Subharmonics and Ultraharmonics in The Forced Oscillations of Weakly Nonlinear Systems." American Journal of Physics Vol. 44 No. 6 1976

[25] Kraftmakher, Y. "magnetic Field of A Dipole And the Dipole-Dipole Interaction," Eur. J. Phys. 2007; 28, 409